

Evidence for a $1g_{9/2}$ rotational band in ^{51}Mn

J. Ekman,¹ D. Rudolph,¹ C. Fahlander,¹ I. Ragnarsson,² C. Andreoiu,^{1,*} M. A. Bentley,³ M. P. Carpenter,⁴ R. J. Charity,⁵ R. M. Clark,⁶ M. Cromaz,⁶ P. Fallon,⁶ E. Ideguchi,^{5,†} A. O. Macchiavelli,⁶ M. N. Mineva,¹ W. Reviol,⁵ D. G. Sarantites,⁵ D. Seweryniak,⁴ V. Tomov,⁵ and S. J. Williams³

¹*Department of Physics, Lund University, S-22100 Lund, Sweden*

²*Department of Mathematical Physics, Lund Institute of Technology, S-22100 Lund, Sweden*

³*School of Chemistry and Physics, Keele University, Keele, Staffordshire ST5 5BG, United Kingdom*

⁴*Physics Division, Argonne National Laboratory, Argonne, Illinois 60439*

⁵*Chemistry Department, Washington University, St. Louis, Missouri 63130*

⁶*Nuclear Science Division, Lawrence Berkeley National Laboratory, Berkeley, California 94720*

(Received 29 August 2002; published 12 November 2002)

A terminating rotational band has been identified in ^{51}Mn following the $^{28}\text{Si}(^{32}\text{S},2\alpha 1p)^{51}\text{Mn}$ fusion-evaporation reaction at 130 MeV beam energy. Spins and tentative positive parities of the band members are assigned based on angular distribution and correlation measurements of transitions, which connect the rotational structure with previously known yrast states. Configuration-dependent cranked Nilsson-Strutinsky calculations suggest a configuration of the band, which comprises one particle in the $1g_{9/2}$ intruder orbit.

DOI: 10.1103/PhysRevC.66.051301

PACS number(s): 21.60.Cs, 23.20.En, 23.20.Lv, 27.40.+z

Nuclei throughout the $1f_{7/2}$ shell exhibit a wide range of phenomena. Nuclei in the vicinity of the doubly magic $N=Z$ nuclei ^{40}Ca and ^{56}Ni are well described by spherical shell model calculations. On the contrary, $N\sim Z$ nuclei near the center of the shell, ^{48}Cr , exhibit a rotational behavior based on significant ground state deformations of $\beta_2\geq 0.3$ [1–3]. Typically, the high-spin spectroscopy of nuclei in the $1f_{7/2}$ shell is established up till noncollective oblate or spherical terminating states, which have spins given either by the number of aligned $1f_{7/2}$ particles relative to ^{40}Ca or the number of aligned $1f_{7/2}$ holes with respect to ^{56}Ni [4]. More recently a few states beyond these terminating points could be identified in heavier $1f_{7/2}$ nuclei. They appear to be of spherical nature, and their main components of the wave functions comprise particles in the upper fp shell [2,5,6].

In ^{56}Ni and nuclei in the vicinity, highly- and superdeformed rotational bands have been observed [7–12], which are mainly based upon four-particle, four-hole excitations across the shell gap at particle number 28 and a number of particles moving in the $1g_{9/2}$ intruder shell. The question arises whether comparable structures may become yrast at high excitation energies in nuclei near the middle of the $1f_{7/2}$ shell, because the $1g_{9/2}$ shell is strongly deformation driving and becomes quickly favored at high rotational frequencies. We provide the first evidence for such a $1g_{9/2}$ rotational band in the nucleus $^{51}\text{Mn}_{26}$, which in addition reveals the characteristics of a favored band termination [13].

In the course of previous high-spin investigations of ^{51}Mn [14–17], the $I^\pi=27/2^-$ terminating state has been reached, for which the spins of the five $1f_{7/2}$ holes relative to the ^{56}Ni core are completely aligned. Spins and parities for the states up to the terminating state have been well determined, and the $17/2^-$ state has been found to be isomeric [17,18].

The present work is based on data from two experiments. The first experiment was performed in 1999 at the Argonne Tandem-Linac Accelerator System (ATLAS). The subsequent experiment was performed in 2001 at the Lawrence Berkeley National Laboratory using a beam from the 88-Inch Cyclotron. Both experiments employed the $^{28}\text{Si}(^{32}\text{S},2\alpha 1p)^{51}\text{Mn}$ fusion-evaporation reaction at 130 MeV beam energy. Enriched 0.5 mg/cm^2 ^{28}Si targets supported with either $\sim 1\text{ mg/cm}^2$ Ta or Au foils were used. The support foils were directed towards the incoming ^{32}S beam. Due to the respective energy loss, the beam energy was effectively ~ 122 MeV at midtarget. The γ rays were detected in the Gammasphere array [19], which comprised 78 Ge-detectors. The Heavimet collimators were removed to allow for γ -ray multiplicity and sum-energy measurements [20]. For the detection of light charged particles the 4π CsI-array Microball [21] was used. The Neutron Shell [22] replaced the four most forward rings of Gammasphere to enable the detection of evaporated neutrons. This allows for the investigation of weak reaction channels at or beyond the $N=Z$ line.

The events were sorted off-line into various E_γ projections, E_γ - E_γ matrices, and E_γ - E_γ - E_γ cubes subject to appropriate evaporated particle conditions. To improve the γ -ray energy resolution an event-by-event kinematic reconstruction method was used to reduce the effect of Doppler broadening caused by the evaporated particles.

The evaporation of two α particles and one proton precedes the population of excited states in ^{51}Mn ($2\alpha 1p$ channel). The relative experimental fusion-evaporation cross section of ^{51}Mn amounts to $\sim 18\%$, and is thus one of the strongest reaction channels. The level scheme of ^{51}Mn is derived from matrices and cubes in coincidence with either two detected α particles and one proton or two α particles and zero or one proton, both with and without additional total energy and multiplicity requirements [23]. The choice has been made depending on whether maximum statistics or cleanest possible spectra set the priority for the given analy-

*Present address: Oliver Lodge Laboratory, University of Liverpool, Liverpool L69 3BX, U.K.

†Present address: RIKEN, Saitama 351-0198, Japan.

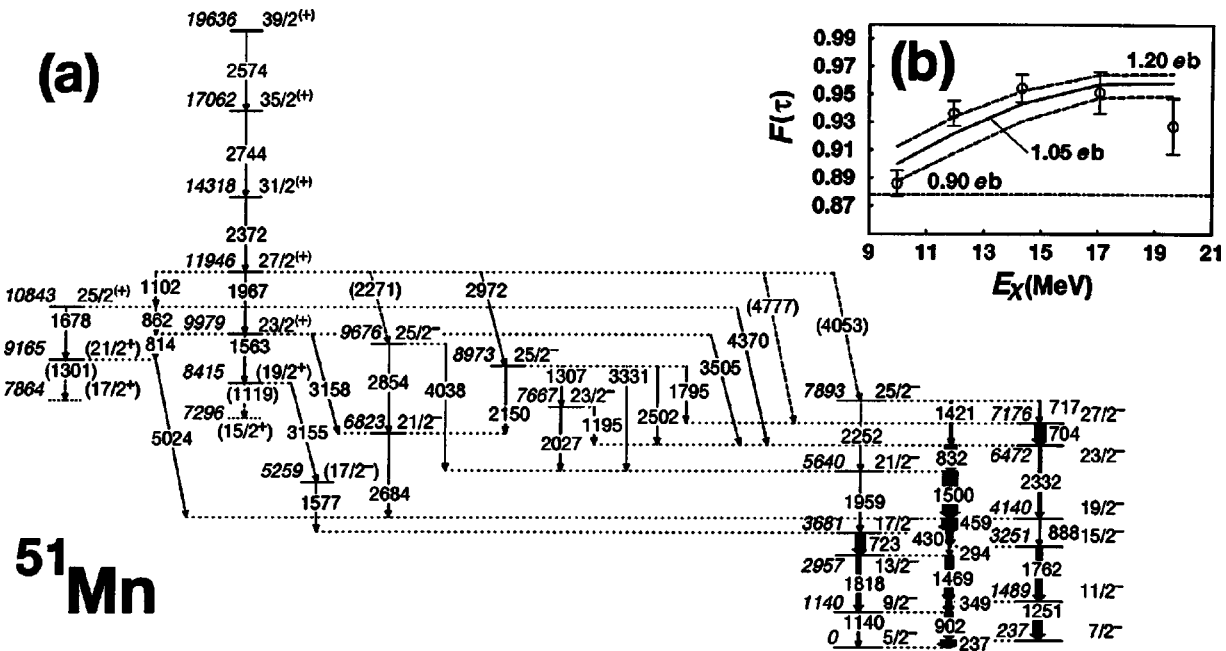


FIG. 1. The proposed level scheme of ^{51}Mn . Energy labels are given in keV. Tentative transitions and levels are dashed. The widths of the arrows represent relative γ -ray intensities. Panel (b) shows experimental and simulated $F(\tau)$ -values vs excitation energy for the rotational structure. The dash-dotted line corresponds to the $F(\tau)$ -value of states decaying outside the target.

sis technique. Possible background transitions arise from the weak 2α channel, ^{52}Fe , but mainly from the $2\alpha 2p$ channel, ^{50}Cr , which leaks into the above mentioned particle gates if one or two protons escaped detection in Microball.

Multipolarity assignments of γ -ray transitions are based on two methods. The 78 Ge-detectors of Gammasphere were grouped into two “pseudo” rings corresponding to average angles $\bar{\theta}=150^\circ$ (15 detectors), and $\bar{\theta}=97^\circ$ (28 detectors). For more details concerning such grouping, see Ref. [6]. Intensity ratios, R_{150-97} , have been determined from spectra taken at either $\bar{\theta}=150^\circ$ or $\bar{\theta}=97^\circ$ in coincidence with transitions detected at an average angle $\bar{\theta}=124^\circ$, where the γ -ray yields are by and large independent of their multipolarity. Stretched $E2$ transitions reveal $R_{150-97}\approx 1.2$, whereas for stretched $\Delta I=1$ transitions $R_{150-97}\approx 0.8$. Secondly, directional correlations of oriented states (DCO-ratios) defined as

$$R_{DCO} = \frac{I(\gamma_1 \text{ at } 150^\circ; \text{gated with } \gamma_2 \text{ at } 97^\circ)}{I(\gamma_1 \text{ at } 97^\circ; \text{gated with } \gamma_2 \text{ at } 150^\circ)} \quad (1)$$

have also been deduced. Known stretched $E2$ transitions were used for gating. $R_{DCO}=1.0$ is expected for observed stretched $E2$ transitions and $R_{DCO}\approx 0.6$ for pure stretched $\Delta I=1$ transitions.

Figure 1(a) shows the relevant part of a largely extended level scheme of ^{51}Mn [24]. Table I lists the information collected for levels and γ -ray transitions in the present work. Most of the states and transitions in the lower-lying yrast structure [right-hand side of Fig. 1(a)] were previously known. Spins and parities could be assigned all the way up to the terminating $27/2^-$ state at 7176 keV excitation energy

[14–16]. The topmost $25/2^-$ level of the signature $\alpha=+1/2$ sequence is newly seen at 7893 keV. It is connected to the known part of the structure via transitions at 717, 1421, and 2252 keV. Both $R_{150-97}=0.61(2)$ and $R_{DCO}=0.33(4)$ evidence that the 1421 keV transition is of mixed $E2/M1$ nature. The low-lying yrast structure is dominated by couplings of the five $1f_{7/2}$ holes. Excitations beyond the new $25/2^-$ state and the above mentioned $27/2^-$ terminating state imply excitations across the spherical shell gap at particle number 28.

A regular cascade of six γ -ray transitions, one of them tentative, has been established at high excitation energies and angular momenta in ^{51}Mn . Figure 2(a) shows a spectrum in coincidence with intense transitions located below the $19/2^-$ state in the yrast structure and one of the two most intense transitions in the rotational band at 1967 or 2372 keV. The band members are visible at 1119 (tentative), 1563, 1967, 2372, 2744, and 2574 keV. Transitions deexciting the band can be seen at 2684, 2972, and 3158 keV, and in the inset the high-energy lines at 3505, 4370, and 5024 keV. Transitions in the previously known low-lying yrast structure are also labeled. Figure 2(b) shows a spectrum in coincidence with the 1563 keV transition and one of the higher lying band members. The tentative 1119 keV transition can be seen as well as the 1577–3155 keV decay path of the level at 8415 keV. In Fig. 2(a) the 3155 keV line is hidden under the stronger 3158 keV transition depopulating the 9979 keV state.

The R_{150-97} and DCO-ratios for the 1967, 2372, 2744, and 2574 keV transitions in the band structure are consistent with stretched quadrupole character. The connecting 3158 and 2684 keV transitions are clearly of dipole nature, and thus the highest observed level at 19636 keV is assigned spin $I=39/2$. The small numbers for R_{150-97} and R_{DCO} of the

TABLE I. The energies of excited states in ^{51}Mn , the transition energies and relative intensities of the γ rays, angular distribution ratios, the DCO-ratios, and spins and parities of the initial and final states of the γ rays.

E_x	E_γ	I_{rel}	R_{150-97}	R_{DCO}	Mult.	I_i^π	I_f^π
237.4(4)	237.4(3)	99.1(30)	0.68(3)	0.55(2)	$E2/M1$	$7/2^-$	$5/2^-$
1139.8(4)	902.4(4)	47.7(14)	0.90(3)	0.68(3)	$E2/M1$	$9/2^-$	$7/2^-$
	1139.7(5)	4.5(2)	1.25(4)	0.86(14)	$E2$	$9/2^-$	$5/2^-$
1488.5(5)	348.8(3)	29.1(9)	0.66(3)	0.55(3)	$E2/M1$	$11/2^-$	$9/2^-$
	1251.1(6)	52.8(16)	0.95(3)	0.80(4)	$E2$	$11/2^-$	$7/2^-$
2957.3(6)	1468.8(7)	43.9(14)	0.90(3)	0.78(3)	$E2/M1$	$13/2^-$	$11/2^-$
	1817.5(8)	23.0(7)	0.92(3)	0.74(4)	$E2$	$13/2^-$	$9/2^-$
3250.8(6)	293.5(3)	2.9(1)	0.56(2)	0.41(8)	$E2/M1$	$15/2^-$	$13/2^-$
	1762.2(8)	39.1(12)	1.05(4)	0.79(4)	$E2$	$15/2^-$	$11/2^-$
3680.6(7)	430.1(3)	34.7(11)	0.52(2)	0.40(2)	$E2/M1$	$17/2^-$	$15/2^-$
	723.2(4)	59.7(18)	0.95(4)	0.78(3)	$E2$	$17/2^-$	$13/2^-$
4139.7(7)	459.2(2)	100.0(30)	0.66(3)	0.52(2)	$E2/M1$	$19/2^-$	$17/2^-$
	888.4(5)	0.9(1)			$E2$	$19/2^-$	$15/2^-$
5258.5(19)	1577(2)	0.2(1)			($\Delta I=0$)	($17/2^-$)	$17/2^-$
5640.0(8)	1500.0(6)	86.5(26)	0.54(2)	0.44(2)	$E2/M1$	$21/2^-$	$19/2^-$
	1959.3(7)	1.2(1)	1.23(4)	0.95(23)	$E2$	$21/2^-$	$17/2^-$
6471.6(8)	831.8(4)	72.3(22)	0.65(3)	0.51(2)	$E2/M1$	$23/2^-$	$21/2^-$
	2332.0(8)	16.7(5)	1.34(5)	1.01(5)	$E2$	$23/2^-$	$19/2^-$
6822.5(10)	2683.6(9)	1.8(3)	0.42(3)	0.29(8)	$E2/M1$	$21/2^-$	$19/2^-$
7176.0(9)	704.4(4)	65.1(20)	1.28(5)	0.95(4)	$E2$	$27/2^-$	$23/2^-$
7666.7(9)	1195.4(6)	0.5(1)			$\Delta I=0$	$23/2^-$	$23/2^-$
	2026.6(7)	1.4(3)	0.44(3)		$E2/M1$	$23/2^-$	$21/2^-$
7892.5(9)	716.8(6)	4.4(2)			$E2/M1$	$25/2^-$	$27/2^-$
	1420.9(6)	7.9(3)	0.61(2)	0.33(4)	$E2/M1$	$25/2^-$	$23/2^-$
	2251.8(10)	0.4(2)			$E2$	$25/2^-$	$21/2^-$
8415.4(20)	1119(2)	0.1(1)			($E2$)	($19/2^+$)	($15/2^+$)
	3155(3)	0.2(1)			($E1$)	($19/2^+$)	($17/2^-$)
8973.0(10)	1307.0(10)	0.3(1)			$E2/M1$	$25/2^-$	$23/2^-$
	1795(2)	0.2(1)			$E2/M1$	$25/2^-$	$27/2^-$
	2150.4(10)	0.2(1)			$E2$	$25/2^-$	$21/2^-$
	2501.8(10)	1.9(2)	0.64(3)	0.49(13)	$E2/M1$	$25/2^-$	$23/2^-$
	3331.3(16)	0.3(1)			$E2$	$25/2^-$	$21/2^-$
9165.3(14)	1301(2)	<0.1			($E2$)	($21/2^+$)	($17/2^+$)
	5024(4)	0.1(1)			($E1$)	($21/2^+$)	$19/2^-$
9676.1(13)	2853.5(11)	0.3(1)	1.56(12)		$E2$	$25/2^-$	$21/2^-$
	4038(3)	0.6(2)	1.49(9)		$E2$	$25/2^-$	$21/2^-$
9979.3(12)	814(1)	0.1(1)			($E2/M1$)	$23/2^{(+)}$	($21/2^+$)
	1563(2)	0.2(1)			($E2$)	$23/2^{(+)}$	($19/2^+$)
	3158.3(12)	0.4(1)	0.65(7)	0.62(8)	($E1$)	$23/2^{(+)}$	$21/2^-$
	3505(3)	0.1(1)			$\Delta I=0$	$23/2^{(+)}$	$23/2^-$
10843.4(12)	862(2)	0.2(1)			($E2/M1$)	$25/2^{(+)}$	$23/2^{(+)}$
	1678(2)	0.2(1)			($E2$)	$25/2^{(+)}$	($21/2^+$)
	4369.9(15)	0.5(1)	0.80(6)		($E1$)	$25/2^{(+)}$	$23/2^-$
11946.0(11)	1102.3(5)	0.2(1)	1.27(13)		($E2/M1$)	$27/2^{(+)}$	$25/2^{(+)}$
	1967.3(8)	0.6(1)	1.59(12)	1.07(13)	$E2$	$27/2^{(+)}$	$23/2^{(+)}$
	2271(2)	<0.1			($E1$)	$27/2^{(+)}$	$25/2^-$
	2972(2)	0.1(1)			($E1$)	$27/2^{(+)}$	$25/2^-$
	4053(4)	<0.1			($E1$)	$27/2^{(+)}$	$25/2^-$
	4777(4)	<0.1			$\Delta I=0$	$27/2^{(+)}$	$27/2^-$
14318.2(16)	2372.2(11)	0.9(2)	1.37(10)	0.97(10)	$E2$	$31/2^{(+)}$	$27/2^{(+)}$
17061.8(20)	2743.6(11)	0.4(1)	1.42(14)	1.16(16)	$E2$	$35/2^{(+)}$	$31/2^{(+)}$
19635.8(28)	2574(2)	0.2(1)	1.64(25)		$E2$	$39/2^{(+)}$	$35/2^{(+)}$

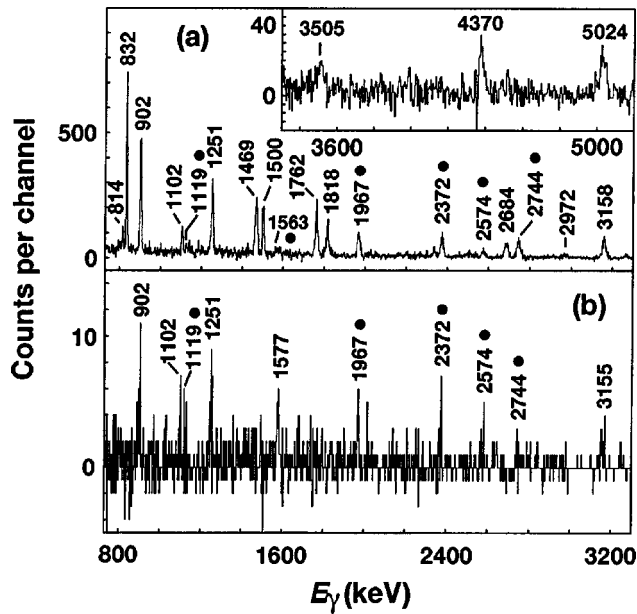


FIG. 2. Panel (a) shows two γ -ray spectra in coincidence with one of the intense transitions below the $19/2^-$ state in the yrast structure and with either the 1967 or 2372 keV transition (main part) or with one of the 1102, 1678, or 1967 keV transitions (inset). The spectrum in panel (b) is measured in coincidence with the 1563 keV transition and one of the other members of the rotational band at either 1967, 2372, 2574, or 2744 keV. The members of the rotational band are marked with filled circles.

2684 keV transition (cf. Table I) can only be explained by a mixed $E2/M1$ character. This yields the spin and parity assignment of $I^\pi=21/2^-$ to the 6823 keV level. A parity changing $E1$ transition is expected to have a mixing ratio close to zero. This makes the 3158 keV transition a good $E1$ candidate since both its R_{150-97} and DCO-ratio are consistent with a pure stretched dipole transition, i.e., positive parity is tentatively assigned to the states in this signature $\alpha=-1/2$ rotational band.

Another interesting feature is the existence of a part of a possible signature $\alpha=+1/2$ band, which is indicated on the left hand side of Fig. 1(a). Unfortunately, it is not feasible to obtain the intensity- or DCO-ratio for the 1678 keV transition. However, a sequence of possibly mixed $E2/M1$ transitions at 814, 862, and 1102 keV is observed, which connect the 9165 and 10843 keV levels with the $\alpha=-1/2$ band. In coincidence with the 814 keV transition we also observe a weak transition at 1301 keV. Similar to the 3158 keV transition mentioned above the 4370 keV line has likely $E1$ character. It depopulates the 10843 keV level. The spins and parities of the 7667, 8973, and 9676 keV states can be fixed based on the analyses of the 2027, 2502, 2854, and 4038 keV transitions, respectively. Other tentative spin and parity assignments of the new levels are based on yrast and intensity considerations and/or the presumed rotational structure.

Using the residual Doppler shift method [25], we deduced an average transition quadrupole moment of $\overline{Q}_t = 1.05(15)eb$ for the band [see Fig. 1(b)]. This corresponds to a quadrupole deformation of $\beta_2 \sim 0.25$ assuming an axially symmetric rotor. Details on the simulation can be found

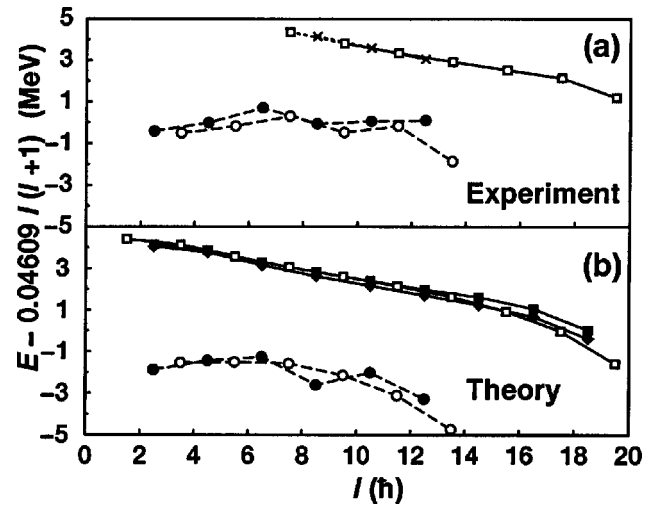


FIG. 3. Panel (a) shows experimental level energies of the two low-spin yrast bands and the newly identified high-spin structures. Dotted lines represent tentative transitions. Dashed (full) lines indicates negative (positive) parity and open (filled) symbols indicate the signature quantum number $\alpha=-1/2$ ($\alpha=+1/2$). Panel (b) provides results of a configuration-dependent cranked Nilsson-Strutinsky calculation. The calculated positive-parity bands represent the $[30,31]$ (open squares), $[41,20]$ (filled diamonds), and $[3+,31]$ (filled squares) configurations. See text for details.

in Refs. [12,24]. A systematic error of $\sim 20\%$ arises from uncertainties in stopping powers, and target and support-foil thicknesses. It is, however, clear that the transitions in the rotational cascade are considerably faster than the 1500 and 2332 keV transitions belonging to the yrast structure, which both have $F(\tau)=0.880(4)$. The lowering in $F(\tau)$ for the 2574 keV transition is consistent with what one would expect for a band termination.

It is interesting to note that the maximum spin, which can be created by having one neutron (proton) in the $1g_{9/2}$ intruder orbit and six holes in the $1f_{7/2}$ shell, is $39/2$ ($37/2$). The lowering in energy of the last observed transition indicates a favored band termination at exactly this spin value. Such configurations would have positive parity, which is consistent with experiment.

The experimental level energies of the high-spin rotational structures are compared with predictions from a configuration dependent cranked Nilsson-Strutinsky calculation [26,13] in Fig. 3. The two negative-parity signature partner bands are included as well. The configurations of the bands are labeled as $[p_1p_2, n_1n_2]$, where p_1 (n_1) denotes the number of proton (neutron) holes in $1f_{7/2}$ orbits and p_2 (n_2) counts the number of $1g_{9/2}$ protons (neutrons). For further details concerning the calculations see, e.g., Refs. [12,13].

Although the absolute and relative energies differ by 1 or 2 MeV, the overall trends in Fig. 3 are in good agreement. Especially the observed favored band termination of the $(\pi, \alpha)=(+, -1/2)$ band is very well reproduced by the predicted $[30,31]$ band [open squares in Fig. 3(b)]. The predicted averaged intrinsic quadrupole moment for the observed levels in the cascade is $\overline{Q}_0 \sim 0.8 eb$, which is somewhat lower, but close to the experimental value. Since

the experimental parities of the band are only tentative, one could also consider configurations which are not based on $1g_{9/2}$ particles, but instead have at least two particles in the upper fp shell. However, calculations for such configurations, e.g., $[40,40]$ or $[30,40]$, show that they are either predicted at too high excitation energy ($[40,40]$), or do not reproduce the observed favored band termination ($[30,40]$).

To spell out the signatures of the odd numbers of $1f_{7/2}$ holes and $1g_{9/2}$ particles, the $[30,31]$ configuration would read $[3_{-0,3_{-1}+}]$. There are three possibilities to change the signature of this configuration to explain the weak $(\pi, \alpha) = (+, +1/2)$ side structure [crosses in Fig. 3(a)]: To move the $1g_{9/2}$ neutron into the first orbital with negative signature ($[30,31_{-}]$), or to change the signature of either a proton or a neutron hole in the $1f_{7/2}$ orbitals ($[3_{+0,31}]$ or $[30,3_{+1}]$ configurations). While the first one requires too much excitation energy [12], the latter two are almost degenerate with the $[30,31]$ band at low spin and a few hundred keV unfavored at higher spin values [cf. filled squares in Fig. 3(b)]. However, the band with the $\alpha = +1/2$ configuration $[41,20]$, i.e., one proton in the lowest $1g_{9/2}$ orbit, is predicted some 300 to 500 keV below the above mentioned signature $\alpha = +1/2$ bands over the whole spin range. It is included in Fig. 3(b) as filled

diamonds. The fact that this configuration involves a $1g_{9/2}$ proton may also provide an explanation for the absence of the $29/2^{+}$, $33/2^{+}$, and $37/2^{+}$ states in the $\alpha = +1/2$ band in Fig. 1, because a 1.3 MeV prompt proton decay [8] from the $29/2^{+}$ state into the 10^{+} yrast state in ^{50}Cr is possible. The absence of the high-spin states in the $\alpha = +1/2$ band can also be explained by the signature splitting, which is predicted between each of the three $\alpha = +1/2$ configurations considered and the $\alpha = -1/2$ $[30,31]$ configuration.

In summary, we have observed a deformed band at high spin in the odd-even $N=Z+1$ nucleus ^{51}Mn . Based on cranked Nilsson-Strutinsky calculations the $\alpha = -1/2$ band is interpreted as one neutron in the $1g_{9/2}$ orbit coupled to a ^{50}Mn core ($[30,31]$ configuration). It is observed up to termination at $I=39/2 \hbar$ and marks the first observation of its kind near the middle of the $1f_{7/2}$ shell.

We would like to thank the accelerator crews and the Gammasphere support staff at Argonne and Berkeley for their supreme efforts. This work was supported in part by the Swedish Natural Science Research Councils and the U.S. Department of Energy under Grants No. DE-AC03-76SF00098 (LBNL), DE-FG05-88ER-40406 (WU), and W-31-109-ENG38 (ANL).

-
- [1] J.A. Cameron *et al.*, Phys. Rev. C **49**, 1347 (1994).
 [2] S.M. Lenzi *et al.*, Z. Phys. A **354**, 117 (1996).
 [3] F. Brandolini *et al.*, Nucl. Phys. **A642**, 387 (1998).
 [4] A. Juodagalvis and S. Åberg, Phys. Lett. B **428**, 227 (1998).
 [5] S.M. Lenzi *et al.*, Phys. Rev. C **56**, 1313 (1997).
 [6] D. Rudolph *et al.*, Eur. Phys. J. A **4**, 115 (1999).
 [7] C.E. Svensson *et al.*, Phys. Rev. Lett. **79**, 1233 (1997).
 [8] D. Rudolph *et al.*, Phys. Rev. Lett. **80**, 3018 (1998).
 [9] C.E. Svensson *et al.*, Phys. Rev. Lett. **82**, 3400 (1999).
 [10] D. Rudolph *et al.*, Phys. Rev. Lett. **82**, 3763 (1999).
 [11] W. Reviol *et al.*, Phys. Rev. C **65**, 034309 (2002).
 [12] C. Andreiou *et al.*, Eur. Phys. J. A **14**, 317 (2002).
 [13] A.V. Afanasjev, D.B. Fossan, G.J. Lane, and I. Ragnarsson, Phys. Rep. **322**, 1 (1999).
 [14] J.W. Noe *et al.*, Nucl. Phys. **A277**, 137 (1977).
 [15] G. Fortuna *et al.*, Nucl. Phys. **A299**, 479 (1978).
 [16] J.A. Cameron *et al.*, Phys. Rev. C **44**, 2358 (1991).
 [17] J. Ekman *et al.*, Eur. Phys. J. A **9**, 13 (2000).
 [18] J. W. Noe and P. Gural, in International Conference on Medium-Light Nuclei, edited by P. Blasi and R. A. Ricci, Florence, Italy, 1978, p. 459.
 [19] I.-Y. Lee, Nucl. Phys. **A520**, 641c (1990).
 [20] M. Devlin *et al.*, Nucl. Instrum. Methods Phys. Res. A **383**, 506 (1996).
 [21] D.G. Sarantites *et al.*, Nucl. Instrum. Methods Phys. Res. A **381**, 418 (1996).
 [22] D. G. Sarantites *et al.* (to be published).
 [23] C.E. Svensson *et al.*, Nucl. Instrum. Methods Phys. Res. A **396**, 228 (1997).
 [24] J. Ekman *et al.* (to be published).
 [25] B. Cederwall *et al.*, Nucl. Instrum. Methods Phys. Res. A **354**, 591 (1995).
 [26] T. Bengtsson and I. Ragnarsson, Nucl. Phys. **A436**, 14 (1985).